Journal of Materials Chemistry A

Accepted Manuscript

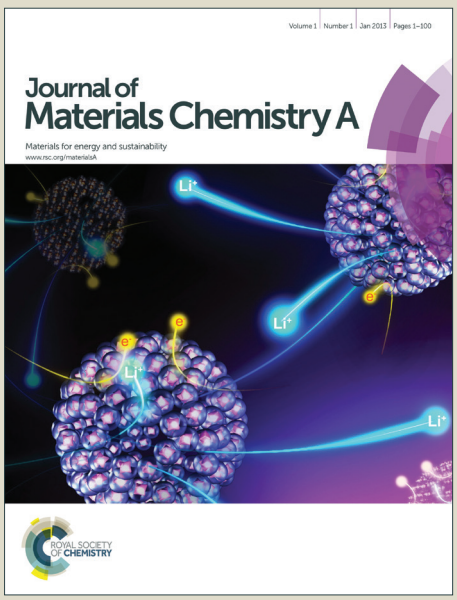

ROYAL SOCIETY OF CHEMISTRY

www.rsc.org/materialsA

Cite this: DOI: 10.1039/c0xx00000x

www.rsc.org/xxxxxx

ARTICLE TYPE

Low-cost and high energy density asymmetric supercapacitors based on polyaniline nanotubes and MoO_3 nanobelts

Hui Peng,[a] Guofu Ma,*[a] Jingjing Mu,[a] Kanjun Sun[b] and Ziqiang Lei*[a]

Received (in XXX, XXX) Xth XXXXXXXXX 20XX, Accepted Xth XXXXXXXXX 20XX

DOI: 10.1039/b000000x

Asymmetric supercapacitors (ASCs) with high energy density are assembled based on pseudocapacitance in both electrodes, which is using polyaniline (PANI) nanotubes as a positive electrode and MoO_3 nanobelts as a negative electrode in 1 M H_2SO_4 aqueous electrolyte. The assembled novel PANI//MoO_3 ASCs device with an extended operating voltage window of 2.0 V in spite of the use of aqueous electrolyte and exhibits excellent performance such as a high specific capacitance of 518 F g^{-1} at a current density of 0.5 A g^{-1}, reaching an energy density as high as 71.9 Wh kg^{-1} at a power density of 254 W kg^{-1} and good cycling stability.

Recently, there has been an increasing demand for environmentally friendly and high-performance energy storage devices[1-2]. Among the various energy storage technologies, supercapacitors (SCs) have attracted much attention due to their high power density and exceptionally long cycle life[3-5]. However, the energy density of commercially available supercapacitors is still lower compared with batteries and fuel cells[6-8]. Therefore, a great deal of recent research effort has been placed on improving the energy density of supercapacitors while maintaining their intrinsic high power density. Actually, the energy density (E) is usually limited to the device capacitance (C) and the operating voltage (V) according to the equation $E = 1/2CV^2$. Therefore, in order to achieve large E, both C and V are needed to increase. At present, most products use organic electrolytes in symmetric/asymmetric supercapacitors to achieve a wider operation voltage while their low capacitance and unfriendly electrolyte undermine their overall effectiveness for supercapacitor applications[9-10]. In fact, aqueous electrolytes have significant inherent advantages over organic electrolytes, such as low cost, high ionic conductivity, large specific capacitance, inherently safe and more environmentally friendly[11-13].

In comparison to symmetric supercapacitors, asymmetric supercapacitors (ASCs) design is an effective approach for extending the operating voltage window and provides higher energy in aqueous electrolytes due to it usually in combination with a battery type (Faradaic) electrode and a capacitor type (electrochemical double layer) electrode to exhibit two different potential windows in the same electrolyte[14-15]. Intensive efforts have been devoted to explore various ASCs systems, such as CoO@polypyrrole//activated carbon[11], MnO_2//graphene[16], graphene-$Ni(OH)_2$//graphene[17] and activated carbon//MoO_3[18]. While most of ASCs devices are commonly use carbon materials as negative or positive materials, it is largely restricts the improvement of energy density due to the unsatisfactory capacitive performance of those materials. However, the study found that the ASCs based on pseudocapacitance in both electrodes can be enhancing the capacitance and energy density[14, 19-21]. Chang et al. developed a ASCs device with reduced graphene oxide (RGO)/MnO_2 composite as a positive electrode and a RGO/MoO_3 composite as a negative in aqueous electrolyte[14]. The operation voltage is expanded to 2.0 V, revealing a high energy density of 42.6 Wh kg^{-1} at a power density of 276 W kg^{-1} and a maximum specific capacitance of 307 F g^{-1} (at 0.2 A g^{-1}). Despite these tremendous achievements, the realization of low-cost, ASCs with high specific energy and power density is still challenging.

In this work, we focused on enhancing the capacitance and energy density of ASCs based on pseudocapacitance in both electrodes, which is using polyaniline (PANI) nanotubes as a positive electrode and MoO_3 nanobelts as a negative electrode in 1 M H_2SO_4 aqueous electrolyte. The PANI with special morphology is generally considered suitable for supercapacitors because of its low cost, high energy density, environmental friendliness and easy synthesis[22-23]. Transition-metal oxides also show high specific capacity toward to supercapacitors when the particle size is decreased to nanoscale[24]. Molybdenum oxide (MoO_3) is an attractive among various transition metal oxides due to its rich, with multiple valence states, and their high electrochemical activity for Li-ion batteries and supercapacitors[25-27]. Based on the difference of working potential window between PANI and MoO_3, the hybrid nanostructure ASCs (PANI//MoO_3) can extended operating voltage window up to 2.0 V in 1 M H_2SO_4 aqueous electrolyte with a specific capacitance of 518 F g^{-1} at a current density of 0.5 A g^{-1}, reaching an energy density as high as 71.9 Wh kg^{-1} at a power density of 254 W kg^{-1}.

The MoO_3 nanobelts were synthesized via a simple low-temperature (140 °C) hydrothermal without any surfactant and template. The morphology and structure of MoO_3 nanobelts are characterized as shown in Figure 1. Figure 1a-b gives the images of as-synthesized MoO_3 exhibits nanobelts morphology on a different magnification. The MoO_3 nanobelts are parallel to each other and indeed form bundles of agglomerated nanobelts with diameters ranging from 100 to 200 nm, and high-magnification image gives more detail of this morphology (Figure 1b). The diffraction peaks of the XRD pattern for the as-synthesized

sample can be clearly indexed to be orthorhombic MoO_3 with preferred orientation (JCPDS No. 05-0508) in Figure 1c. The strong diffraction peaks of (020), (040), and (060) planes reveal a layered crystal structure or a highly anisotropic growth of the oxides[28].

The PANI nanotubes were synthesized via a simple chemical template-free method in the presence of D-tartaric acid as the dopant, and ammonium persulfate as the oxidant. Typical SEM images of the as-synthesized PANI nanotubes are given in Figure 1d. As can be seen, the PANI products take on nanotubes shape and the high magnification (inset in Figure 1d) illustrates that they are tubular structures. In addition, the external surface of these nanotubes is seen to be relatively rough and decorated by some PANI nanoparticles. This interesting structure of PANI nanotubes are further characterized by TEM. It is very obvious that the product of PANI shows the nanotubes structures with 20~50nm in tube diameter, which is in agreement with the result of the SEM. The XRD pattern of PANI nanotubes is shown in Figure 1f. It can be seen that the PANI nanotubes has a primary characteristic peak at 24.8° attributed to the scattering from the periodicity perpendicular to PANI chains and the one at 20.3° to the alternating distance between layers of polymer chains[29].

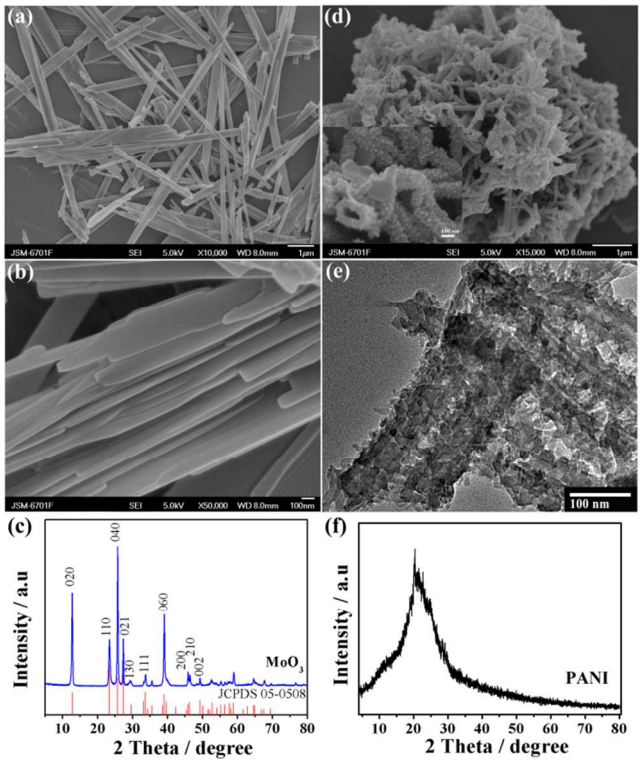

Figure 1. (a, b) SEM images of as-synthesized MoO_3 exhibit nanobelts morphology on a different magnification; (c) XRD pattern of MoO_3 nanobelts; (d) SEM images of PANI exhibits nanotubes morphology (the high magnification insert the figure); (e) TEM image of PANI nanotubes; (f) XRD pattern of PANI nanotubes.

The electrochemical studies for the MoO_3 nanobelts and PANI nanotubes were first performed in a three-electrode cell using aqueous 1 M H_2SO_4 electrolyte. Cyclic voltammetry (CV) is generally used to characterize the capacitive behavior of an eletrode material. Figure 2a-b show the CV curves of MoO_3 nanobelts negative electrode and PANI nanotubes positive electrode at different scan rates, respectively. CV curves of the prepared MoO_3 nanobelts at different scan rates in the potential window of -0.8 to 0 V appear two pairs of redox peaks, which show that the MoO_3 has faradaic pseudocapacitance behavior. These two sets of redox peaks at -0.33/-0.44 V and -0.45/-0.64 V, respectively, which are corresponds to the reversible intercalation/deintercalation of H^+ ions into/out of the MoO_3 host[25,26]. The electrochemical mechanism of MoO_3 in H^+ electrolyte can be expressed as:

$$MoO_3 + xe^- + xH^+ \leftrightarrow H_xMoO_3 \quad (1)$$

$$H_xMoO_3 + ye^- \leftrightarrow H_{x+y}MoO_3 \quad (2)$$

It is observed that CV curve area and the peak current rapidly increase with the increase of the scan rate from 10 to 50 mV s^{-1}. Moreover, two pairs of redox peaks are still clearly observed even at a scan rate of 50 mV s^{-1}. The result reveals that the MoO_3 electrode has the reversible redox processes and good rate ability in aqueous H_2SO_4 electrolyte. All of the PANI nanotubes CV curves at different scan rates are exhibited an ideal rectangular shape with pseudocapacitance characteristics (Figure. 2b). The PANI typical redox peaks can clearly be found on the CV curves at different scan rates in the potential window of -0.2 to 0.8 V. The first couple of peaks (about 0.21/0.10 V) are attributed to the redox transition of PANI between a semi-conducting state (leucoemeraldine form) and a conducting state (polaronicemeraldine form). The peaks at 0.47/0.44 V, 0.55/0.53 V and 0.76/0.70 V are ascribed to the benzo/hydroquinone (BQ/HQ), *p*-aminophenol/benzoquinoneimine (PAP/QI) redox pair and formation/reduction of bipolaronic pernigraniline and protonated quinonediimine, respectively[30].

Typical galvanostatic charge/discharge curves of MoO_3 nanobelts negative electrode and PANI nanotubes positive electrode collected at different current densities are shown in Figure 2c-d, respectively. All discharge curves are almost symmetrical to the corresponding charge curves, indicating good capacitive behavior for these electrodes. The corresponding specific capacitances are calculated from galvanostatic charge/discharge curves and shown in Figure 2e-f. The MoO_3 nanobelts exhibits high specific capacitances of 560 F g^{-1} and 208 F g^{-1} at a current density of 1 A g^{-1} and 10 A g^{-1} , respectively. The high specific capacitance of MoO_3 nanobelts is ascribed to nanobelt morphology. The orthorhombic MoO_3 possesses a unique double-layered structure in (010) direction and the nanobelt morphology is revealed more active crystallographic (010) planes, which is favorable for intercalation and deintercalation of molecules and ions between layers[26]. Therefore, it can provide a great deal of fast electron-transport access to the current collector, allowing for rapid electron transfer from active redox sites to the electrode. Similarly, the specific capacitance value of the PANI nanotubes is calculated as high as 504 F g^{-1} at current density of 1 A g^{-1}. Even at a current density as high as 10 A g^{-1}, the specific capacitance can still achieve to 379 F g^{-1}, which remains approximate to 75% of the initial specific capacitance (Figure 2f). The PANI nanotubes materials present a high capacitance that may attribute to the unique tubular structures, which enhance the kinetics of ion and electron transport in electrodes and at the electrode/electrolyte interface. The electrochemical properties of the electrodes were examined further by electrochemical impedance spectroscopy (EIS). Figure

S1 show Nyquist plots with the semicircle on the real component (Z' axis) in the high-frequency region and the straight sloped line in the low-frequency region both of PANI and MoO_3. The diameter of the semicircle corresponds to the charge-transfer resistance (R_{ct}) caused by Faradic reactions and EDLC (C_{dl}) at the electrode/electrolyte interface. Therefore, the conductivity of PANI is better that of MoO_3 due to PANI has a smaller diameter of the semicircle than MoO_3. Moreover, the phase angle for the impedance plots of PANI and MoO_3 show higher than 45° in the low frequency, suggesting its high capacitive behavior.

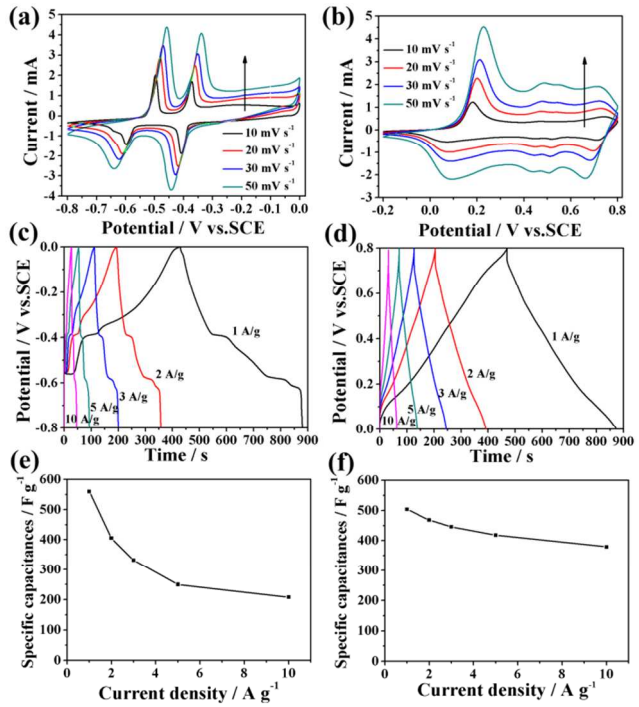

Figure 2. (a, b) CV plots of the MoO_3 and PANI electrodes at various scan rates performed in three electrode cell in 1 M H_2SO_4 electrolyte, respectively; (c, d) Galvanostatic charge/discharge curves of MoO_3 and PANI electrodes at different current densities performed in three electrode cell, respectively; (e, f) Specific capacitance of the MoO_3 and PANI electrodes at different current densities, respectively.

Based on high capacitance of the redox pseudocapacitance properties of MoO_3 and PANI, an asymmetric supercapacitor was fabricated using these materials as the negative and positive electrodes, respectively. The MoO_3 electrode was measured within a potential window of -0.8 to 0 V (vs. SCE), while PANI was performed within a potential window of -0.2 to 0.8 V (vs. SCE) at a scan rate of 20 mV s^{-1} in 1 M H_2SO_4 electrolyte (Figure 3a). Therefore, it is expected that the operating cell voltage can be at least extended to 1.6 V when they are assembled into ASCs. As for a supercapacitor, the charge balance will follow the relationship $q_+ = q_-$, where the charge stored by each electrode usually depends on the specific capacitance (C), the potential range for the charge/discharge process (ΔE), and the mass of the electrode (m) following Equation: $q = C \times \Delta E \times m$ [31]. Thus, in the design cell, the loading mass ratio of active materials (m(PANI) / m(MoO_3)) was estimated to be 0.89 from the specific capacitance calculated from their galvanostatic charge/discharge curves. As shown in Figure 3b, the asymmetric supercapacitor device exhibits capacitive behavior with distorted semirectangular shaped CV curves and the operating voltage up to 2.0 V in 1 M H_2SO_4 electrolyte. The rationality of this operating voltage between PANI and MoO_3 are further tested (Figure S2). In addition, the CV curves also with obvious redox peaks at different scan rates, which indicating pseudocapacitance is generated in asymmetric supercapacitors. The galvanostatic charge/discharge curves of PANI//MoO_3 ASCs at various current densities are shown in Figure 3c. The non-linearity in the charge and discharge curves particularly at lower current density indicates some contribution of the redox reaction from MoO_3 and PANI, which is in agreement with the result of the CV curves. However, the charging and discharging curves are still nearly symmetric, evidencing highly reversible electrochemistry. According to the formula of specific capacitance (Supporting Information), the gravimetric capacitance of PANI//MoO_3 ASCs as high as 518 F g^{-1} at a current density of 0.5 A g^{-1}, which is much higher than recent reports for other ASCs, such as RGO-RuO_2//RGO-PANI (about 360 F g^{-1} at 0.3 A g^{-1})[13], $GrMnO_2$//$GrMoO_3$ (307 F g^{-1} at 0.2 A g^{-1})[14] and $Ni(OH)_2$/UGF//a-MEGO (119 F g^{-1} at 1 A g^{-1})[32]. Furthermore, the PANI//MoO_3 ASCs device shows good rate performance with 53 % of gravimetric capacitance retained when the current density increased from 0.5 to 5 A g^{-1}, which is attributed to the combination of high specific capacitances in both electrodes.

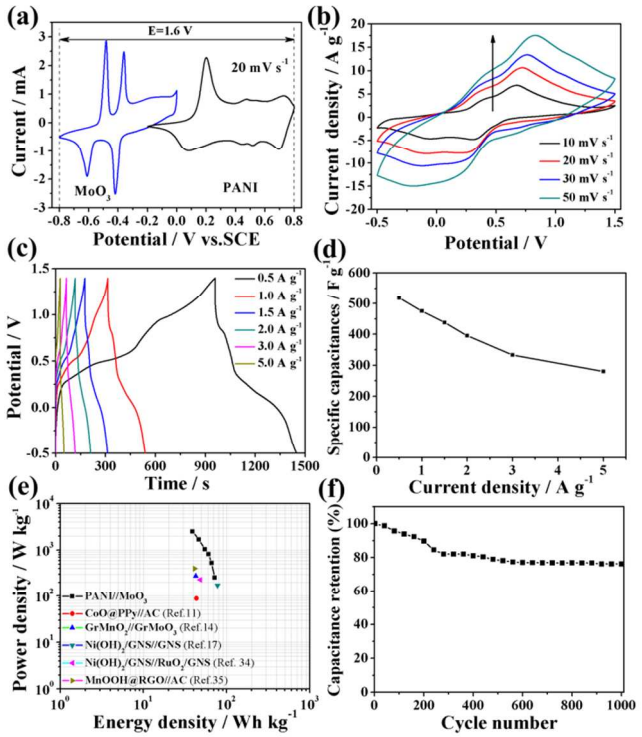

Figure 3. (a) Comparative CV curves of PANI and MoO_3 electrodes performed in three electrode cell in 1 M H_2SO_4 electrolyte at a scan rate of 20 mV s^{-1}; (b) CV curves an PANI//MoO_3 ASCs at different scan rates in 1 M H_2SO_4 electrolyte; (c) Galvanostatic charge/discharge curves of PANI//MoO_3 ASCs at different current densities; (d) Specific capacitance of the ASCs at different current densities; (e) Ragone plot related to energy and power densities of the PANI//MoO_3 ASCs in comparison to asymmetric supercapacitor recently reported in the literature[11, 14, 17, 34-35]; (d) Cycling stability of the PANI//MoO_3 ASCs.

Figure S3 shows Nyquist plot of PANI//MoO_3 ASCs with the

small semicircle in the high-frequency region and the vertical curve in the low-frequency region, which results indicating a low charge-transfer resistance in the electrochemical system and a pronounced capacitive behavior with small diffusion resistance, respectively. The Nyquist plots obtained are modeled and interpreted with the help of an appropriate electric equivalent circuit (the inset of Figure S3), where R_e stands for a combined resistance of ionic resistance of electrolyte, intrinsic resistance of substrate and contact resistance at the active material/current collector interface, R_{ct} the charge tansfer resistance casued by the faradaic reaction. The slope of the 45° portion of the curve is called the Warburg resistance (Z_W) and is a result of the frequency dependence of ion diffusion/transport in the electrolyte to the electrode surface, *CPE* is the constant phase element, C_L is the limit capacitance[14].

Ragone plot of the device describing the relation between energy density and power density was obtained and shown in Figure 3e. The energy and power densities were calculated from the discharge curves at different current densities. It is obviously that the PANI//MoO_3 ASCs exhibit the highest energy density is 71.9 Wh Kg^{-1} with a power density of 254 W Kg^{-1} and remained 38.9 Wh Kg^{-1} at 2500 W Kg^{-1}. Moreover, the obtained maximum energy density is considerably higher than those of recently reported ASCs, such as $GrMnO_2$//$GrMoO_3$ (42.6 Wh kg^{-1})[14], CNT/MnO_2//CNT/In_2O_3 (25.5 Wh kg^{-1})[33] and Ni$(OH)_2$/graphene//RuO_2/graphene (48 Wh kg^{-1})[34]. Table S1 summarizes asymmetric supercapacitors devices from various and Ragone plots are shown in Figure 3e. The excellent performance of ASCs device can be ascribed to the following reasons: 1) PANI nanotubes electrodes exhibit unique tubular porous structures and superior electrical properties, which favor fast ion and electron transportation; 2) the orthorhombic MoO_3 possesses a unique double-layered structure, which is favorable for intercalation and deintercalation of molecules and ions between layers. In addition, we also evaluate the long-term cycle stability of the PANI//MoO_3 ASCs by repeating the galvanostatic charge/discharge test between -0.5 and 1.5 V at a current density of 3 A g^{-1} for 1000 cycles. Figure 3f shows the capacitance retention ratio of the asymmetric supercapacitors charged at 2.0 V as a function of the cycle number. It shows that the PANI//MoO_3 ASCs exhibits electrochemical stability with about 78% retention of the initial available specific capacitance after 1000 cycles. It is worth noting that the specific capacitance sharply decreases after the initial 300 cycles (retained 82.5% of its initial capacitance), which is probably related to the swelling and shrinkage of conducting PANI during the long-term charge/discharge processes.

Conclusions

In summary, high energy density asymmetric supercapacitors (PANI//MoO_3) are fabricated with polyaniline (PANI) nanotubes as a positive electrode and MoO_3 nanobelts as a negative electrode in 1 M H_2SO_4 aqueous electrolyte. Comparing with previously reported ASCs, our novel desgined PANI//MoO_3 ASCs demonstrated excellent performance in a large potential window of 2.0 V and exhibited high specific capacitance of 518 F g^{-1} at a current density of 0.5 A g^{-1}. Meanwhile, the ASCs exhibit an energy density as high as 71.9 Wh kg^{-1} at a power density of 254 W kg^{-1}. These encouraging findings can open up the possibility of cheap conductive polymers and metal oxides for applications in asymmetric supercapacitors with low cost, high energy, and high power densities to meet the diverse demands for next-generation energy storage systems.

Notes and references

[a] *Key Laboratory of Eco-Environment-Related Polymer Materials of Ministry of Education, Key Laboratory of Polymer Materials of Gansu Province, College of Chemistry and Chemical Engineering, Northwest Normal University, Lanzhou 730070, China*
Fax/Tel: +86-931-7975121;
E-mail: magf@nwnu.edu.cn; Leizq@nwnu.edu.cn
[b] *College of Chemistry and Environmental Science, Lanzhou City University, Lanzhou 730070, China*

† Electronic Supplementary Information (ESI) available: [Experimental details and electrochemical measurements. Figure S1-S3 and Table S1]. See DOI: 10.1039/b000000x/

1. M. F. El-Kady, V. Strong, S. Dubin and R. B. Kaner, *Science* 2012, **335**, 1326-1330.
2. H. Jiang, P. S. Lee and C. Li, *Energy Environ. Sci.*, 2013, **6**, 41-53.
3. Z. Chen, Y. Yuan, H. Zhou, X. Wang, Z. Gan, F. Wang and Y. Lu, *Adv. Mater.*, 2014, **26**, 339-345.
4. L. Dai, D. W. Chang, J.-B. Baek and W. Lu, *Small* 2012, **8**, 1130-1166.
5. L. Yuan, B. Yao, B. Hu, K. Huo, W. Chen and J. Zhou, *Energy Environ. Sci.*, 2013, **6**, 470-476.
6. Q. Qu, S. Yang and X. Feng, *Adv. Mater.*, 2012, **23**, 5574-5580.
7. G. Wang, L. Zhang, and J. Zhang, *Chem. Soc. Rev.*, 2012, **41**, 797-828.
8. S. Giri, D. Ghosh and C. K. Das, *Adv. Funct. Mater.*, 2013, **24**, 1312-1324.
9. Y. Zhu, S. Murali, M. D. Stoller, K. J. Ganesh, W. Cai, P. J. Ferreira, A. Pirkle, R. M. Wallace, K. A. Cychosz, M. Thommes, D. Su, E. A. Stach and R. S. Ruoff, *Science* 2011, **332**, 1537-1541.
10. Y. Liang, F. Liang, H. Zhong, Z. Li, R. Fu and D. Wu, *J. Mater. Chem. A*, 2013, **1**, 7000-7005.
11. C. Zhou, Y. Zhang, Y. Li and J. Liu, *Nano lett.*, 2013, **13**, 2078-2085.
12. F. Wang, S. Xiao, Y. Hou, C. Hu, L. Liu and Y. Wu, *RSC Adv.*, 2013, **3**, 13059-13084.
13. J. Zhang, J. Jiang, H. Li and X. S. Zhao, *Energy Environ. Sci.*, 2011, **4**, 4009-4015.
14. J. Chang, M. Jin, F. Yao, T. H. Kim, V. T. Le, H. Yue, F. Gunes, B. Li , A. Ghosh, S. Xie and Y. H. Lee, *Adv. Funct. Mater.*, 2013, **23**, 5074-5083.
15. C. Peng, S. Zhang, X. Zhou and G. Z. Chen, *Energy Environ. Sci.*, 2010, **3**, 1499-1502.
16. H. Gao, F. Xiao, C. B. Ching and H. Duan, *ACS Appl. Mater. Interfaces* 2012, **4**, 2801-2810 .
17. J. Yan, Z. Fan, W. Sun, G. Ning, T. Wei, Q. Zhang, R. Zhang, L. Zhi and F. Wei, *Adv. Funct. Mater.*, 2012, **22**, 2632-2641.
18. W. Tang, L. Liu, S. Tian, L. Li, Y. Yue, Y. Wu and K. Zhu, *Chem. Commun.*, 2011, **47**, 10058-10060.
19. P. Yang, Y. Ding, Z. Lin, Z. Chen, Y. Li, P. Qiang, M. Ebrahimi, W. Mai, C. P. Wong and Z. L. Wang, *Nano lett.*, 2014, **14**, 731-736.
20. J. Xu, Q. Wang, X. Wang, Q. Xiang, B. Liang, D. Chen and G. Shen, *ACS Nano* 2013, **7**, 5453-5462.
21. W. H. Jin, G. T. Cao and J. Y. Sun, *J. Power Sources* 2008, **175**, 686-691.
22. A. Sumboja, C. Y. Foo, J. Yan, C. Yan, R. K. Gupta and P. S. Lee, *J. Mater. Chem.*, 2012, **22**, 23921-23928.
23. H. Cong, X. Ren, P. Wang and S. Yu, *Energy Environ. Sci.*, 2013, **6**, 1185-1191.
24. G. A. Snook, P. Kao and A. S. Best, *J. Power Sources* 2011, **196**, 1-12.
25. R. Liang, H. Cao and D. Qian, *Chem. Commun.*, 2011, **47**, 10305-10307.
26. J. Jiang, J. Liu, S. Peng, D. Qian, D. Luo, Q. Wang, Z. Tian and Y. Liu, *J. Mater. Chem. A*, 2013, **1**, 2588-2594.
27. X. Wang, R. Nesper, C. Villevieille and P. Novák, *Adv. Energy Mater.*, 2013, **3**, 606-614.

28. C. V. Subba Reddy, E. H. Walker Jr, C. Wen and S. Mho, *J. Power Sources* 2008, **183**, 330-333.
29. J. P. Pouget, M. E. Jozefowicz, A. J. Epstein, X. Tang and A. G. MacDiarmid, *Macromolecules* 1991, **24**, 779-789.
30. D. E. Stilwell and S. M. Park, *J. Electrochem. Soc.*, 1988, **135**, 2254-2262.
31. Z. Fan, J. Yan, T. Wei, L. Zhi, G. Ning, T. Li and F. Wei, *Adv. Funct. Mater.*, 2011, **21**, 2366-2375.
32. J. Ji, L. Zhang, H. Ji, Y. Li, X. Zhao, X. Bai, X. Fan, F. Zhang and R. S. Ruoff, *ACS Nano* 2013, **7**, 6237-6243.
33. P. C. Chen , G. Shen , Y. Shi , H. Chen and X. Zhou , *ACS Nano* 2010, **4**, 4403-4411.
34. H. Wang, Y. Liang, T. Mirfakhrai, Z. Chen, H. S. Casalongue and H. Dai, *Nano Res.*, 2011, **4**, 729-736.
35. Y. Cao, Y. Xiao, Y. Gong, C. Wang and F. Li, *Electrochim. Acta* 2014, **127**, 200-207.

ToC Fig